MOLECULAR AND CELLULAR BIOLOGY, Feb. 1988, p. 632–646
0270-7306/88/020632-15$02.00/0
Copyright © 1988, American Society for Microbiology
Vol. 8, No. 2

Elevated Expression of pp60$^{c\text{-}src}$ Alters a Selective Morphogenetic Property of Epithelial Cells In Vitro without a Mitogenic Effect

STEPHEN L. WARREN, LAURA M. HANDEL, AND W. JAMES NELSON*
Institute for Cancer Research, Philadelphia, Pennsylvania 19111

Received 2 September 1987/Accepted 4 November 1987

Madin-Darby canine kidney (MDCK) cells are highly differentiated and have retained the morphogenetic properties necessary to form polarized, multicellular epithelial structures (cysts) in vitro that resemble epithelial tissues in vivo. We introduced the c-*src* gene into MDCK cells to elevate the level of the plasma membrane-associated cellular tyrosine kinase, pp60$^{c\text{-}src}$, to levels two- to ninefold higher than that expressed in parent MDCK cells. Our results revealed a highly discriminatory biological action of pp60$^{c\text{-}src}$ on the morphogenetic properties of MDCK cells. Elevated expression of pp60$^{c\text{-}src}$ conferred on MDCK cells the ability to undergo dramatic changes of cell shape that includes the formation of long cell processes (100 to 200 μm), never observed in control MDCK cells. The morphogenesis of multicellular epithelial cysts was altered by elevated levels of pp60$^{c\text{-}src}$ and led to predictable distortions of their three-dimensional architecture. However, these cells established morphologically normal cell polarity, formed adhesive epithelial cell-cell contacts indistinguishable from those of control MDCK cells, and exhibited neither focus-forming ability or anchorage-independent growth potential. Finally, we showed that MDCK cells expressing elevated levels of pp60$^{c\text{-}src}$ exhibit increased phosphorylation of a more limited number of phosphotyrosine-containing proteins than MDCK cells expressing pp60$^{v\text{-}src}$. We suggest that a natural function of pp60$^{c\text{-}src}$ is to regulate the morphogenetic properties which determine the shape of differentiated cells and multicellular structures.

The cellular tyrosine kinase, pp60$^{c\text{-}src}$, is structurally homologous to the transforming protein of the Rous sarcoma virus, pp60$^{v\text{-}src}$, which induces morphological alterations and uncontrolled proliferation of cells. However, the natural biological function of pp60$^{c\text{-}src}$ is unknown (4, 5, 34, 35, 66, 67).

The c-*src* gene has been assayed for biological activity almost exclusively by transformation assays that detect genes which lead to uncontrolled proliferation of cells (9, 36, 38, 41, 44, 56, 57, 61). Elevated levels of pp60$^{c\text{-}src}$ do not transform chicken or rat fibroblasts in vitro (36, 56), although very high levels of pp60$^{c\text{-}src}$ have weak focus-inducing activity in NIH 3T3 cells (38). Thus, pp60$^{c\text{-}src}$ can partially mimic the transforming action of pp60$^{v\text{-}src}$, but only under exceptional circumstances (34). Since elevated pp60$^{c\text{-}src}$ expression in vivo is most abundant in differentiated cells that cannot divide (15, 21, 45, 64, 71; also see Discussion), it is possible that pp60$^{c\text{-}src}$ has a nonmitogenic natural function which does not manifest itself in transformation assays.

We have developed a simple in vitro biological assay that detects nonmitogenic, morphoregulatory activities of pp60^{src} kinases (72). The assay is based on the ability of Madin-Darby canine kidney (MDCK) cells to establish specific cell-cell contacts and to generate tissuelike multicellular structures (cysts) composed of polarized epithelial monolayers (10, 11, 30, 52, 59, 70). We have shown previously that low-level expression of pp60$^{v\text{-}src}$ in MDCK cells leads to flat, more spread-out cells and disrupts selective cell adhesion components between MDCK cells, but does not have a mitogenic effect (72). Furthermore, multicellular epithelial cysts composed of these cells exhibited architectural deformations only in regions of the cyst wall which were subjected to mechanical stress. These studies suggested to us that low levels of pp60$^{v\text{-}src}$ mimic the action of a related cellular tyrosine kinase, such as pp60$^{c\text{-}src}$. Since an elevation of pp60$^{c\text{-}src}$ levels appears to coincide with dynamic changes in the morphogenetic activities of cells in vivo (see Discussion), we sought to test this idea by elevating pp60$^{c\text{-}src}$ expression above the level of pp60$^{c\text{-}src}$ that exists in control MDCK cells. The results showed that elevated levels of pp60$^{c\text{-}src}$ confer on MDCK cells a capacity for marked changes in cell shape without a mitogenic effect. These cells generate multicellular, polarized epithelial structures that exhibit predictable distortions of their three-dimensional architecture. Our studies showed that areas of the plasma membrane involved in MDCK cell-cell contact are enriched with pp60$^{c\text{-}src}$; however pp60$^{c\text{-}src}$ does not appear to modulate the degree of cell-cell adhesion as shown previously for pp60$^{v\text{-}src}$. Thus, pp60$^{c\text{-}src}$ exhibits a highly discriminatory biological action since it alters a subset of the morphogenetic properties which are altered by pp60$^{v\text{-}src}$. We suggest that a natural function of pp60$^{c\text{-}src}$ is to confer on differentiated cells and multicellular structures the ability to undergo changes in shape without affecting the proliferative status of the cells.

MATERIALS AND METHODS

Vector constructions. The T4 DNA ligase, Klenow fragment of *Escherichia coli* DNA polymerase I, *Bam*HI linker, and all restriction enzymes were purchased from New England BioLabs, Inc. (Beverly, Mass.). The bacterial alkaline phosphatase was from International Biotechnologies, Inc. (New Haven, Conn.).

Details of pFVXMneo, pMv-*src*, and pMOneoMT$_{211}$v-*src* have been described elsewhere (38, 42, 72). pMc-*src*ΔiSVneo was constructed by a five-step procedure, using techniques described previously (49). First, the c-*src*-coding sequence was removed from p5H (provided by H. Hanafusa; see reference 44). The *Nco*I site within the ATG start codon and the *Bgl*II site downstream of the c-*src*-coding sequence were cut to yield a 1.7-kilobase (kb) restriction fragment that was excised and purified from a preparative agarose gel.

* Corresponding author.

Second, the v-*src*-coding sequence was removed from pMv-*src* (provided by D. Shalloway; see reference 38) by partial *Nco*I restriction digestion and complete *Bgl*II restriction digestion. The remaining 6.7-kb vector backbone was gel purified and contained the long terminal repeats (LTRs), a 1.8-kb intron containing 5′ and 3′ splice sites and the ψ site, the plasmid replication origin, and the Amp^r gene. Third, the 1.7-kb *Nco*I-*Bgl*II restriction fragment containing the c-*src*-coding sequence was ligated into the 6.7-kb vector backbone to yield pMc-*src*Δi. The pMc-*src*Δi plasmid lacked transforming activity (data not shown), indicating that v-*src* sequences were successfully removed from Mv-*src* in the second step. Fourth, the *Bgl*II site in pMc-*src*Δi was cut and dephosphorylated. Fifth, a 1.6-kb *Bam*HI restriction fragment from pSVneo4 containing the transposon Tn*5* Neo^r-coding sequence under the control of the simian virus 40 early region enhancer-promoter segment was ligated into the *Bgl*II site of pMc-*src*Δi to generate the completed vector, pMc-*src*ΔiSVneo.

Generation of virus stocks. Virus stocks were prepared from ψAM cells as described previously (14, 72).

Southern analysis. High-molecular-weight DNA was isolated from MDCK cells and cut with *Eco*RI. The digested DNAs (13 μg) were applied to a 1% (wt/vol) agarose gel, electrophoresed, transferred to nitrocellulose paper, and hybridized to nick-translated DNA probes as described previously (49).

Northern (RNA) analysis. RNA was extracted from MDCK cells by the hot-phenol method which is described elsewhere (49). Total RNA (25 μg) from each clone was denatured with formaldehyde and formamide and applied to a 1% formaldehyde-containing agarose gel, electrophoresed, and transferred to nitrocellulose paper, hybridized, washed, and exposed as described previously (49). For quantitation, a segment of nitrocellulose paper containing both the subgenomic retroviral c-*src* mRNA species and the endogenous c-*src* transcript from each of the lanes 3 to 7 in Fig. 3A and a segment of nitrocellulose paper containing the endogenous c-*src* transcript from lane 2 of Fig. 3A (MFN-2 cells) were cut out and compared by scintillation spectroscopy. The radioactivity (counts per minute) from each band was divided by the radioactivity (counts per minute) of a band corresponding to the RNA transcript of ribosomal protein 32 (provided by R. Perry) which served as an internal standard. The ratio determined for MFN-2 was given an arbitrary value of 1.0, and the other ratios were normalized accordingly.

pp60$^{c\text{-}src}$ kinase assay. The pp60$^{c\text{-}src}$ kinase assay was performed as described previously (13, 72).

Metabolic labeling with $^{32}P_i$. Cells (10^6) of each clone were seeded in 35-mm petri dishes in complete Dulbecco modified Eagle medium with 10% fetal bovine serum. For metabolic labeling, the medium was replaced with 2 ml of phosphate-free minimal essential medium supplemented with 5% dialyzed fetal bovine serum and 1 mCi of $^{32}P_i$ (5 mCi/ml; New England Nuclear/DuPont). The cells were incubated for 15 h at 37°C. The cells were rinsed in ice-cold phosphate-buffered saline (PBS) and extracted for 15 min in 1 ml of ice-cold RIPA buffer (26) at 4°C. The extract was centrifuged at ~12,000 × *g* for 30 min at 4°C, and the supernatant was normalized to total protein content by the Bio-Rad protein assay. Equal volumes of the extract, each containing 550 μg of protein, were incubated with 5 μl of polyclonal antibody which recognizes multiple phosphotyrosine-containing proteins (provided by Carl-Henrik Heldin; see reference 17) for 60 min at 4°C. *Staphylococcus aureus* protein A-Sepharose 4B beads (10 μl; Pharmacia Fine Chemicals, Piscataway, N.J.) were added and rocked at 4°C for 1 h. The beads were washed four times in RIPA buffer, boiled in 70 μl of sodium dodecyl sulfate sample buffer, and applied to 5 to 15% linear gradient polyacrylamide-sodium dodecyl sulfate gel (43). The gel was fixed and stained with Coomassie brilliant blue. After destaining, the gel was dried and exposed to XAR-5 X-ray film for 96 h at −80°C without an intensifying screen.

Cell culture. The MDCK cells used in this study were cloned from an original low-passage-number stock and have been characterized previously (54). Cells were grown in Dulbecco modified Eagle medium supplemented with 10% fetal bovine serum at 37°C in a humidified atmosphere containing 5% CO_2. The focus formation assays and anchorage-independent growth assays were performed as described previously (72). Spherical and disk-shaped multicellular cysts were made as described previously (72).

Electron microscopy and light microscopy. Electron and light microscopy were performed as described previously (72).

Indirect immunofluorescence. Cells were grown on collagen-coated cover slips, fixed with 1.75% (wt/vol) formaldehyde in PBS, washed in PBS for 10 min, and then permeabilized with PBS containing 0.5% (vol/vol) Triton X-100 and 2 mM $MgCl_2$ for 2 to 15 min at room temperature. For double immunofluorescence, mouse monoclonal anti-pp60$^{v\text{-}src}$ antibody (MAb 327) (provided by J. Brugge; see reference 46) and the rabbit antiactin antibodies (54) were mixed and diluted 1:10 and incubated with the fixed cells. After the cells were washed with PBS, affinity-purified goat anti-mouse immunoglobulin G (IgG) conjugated to rhodamine (Boehringer Mannheim Biochemicals, Indianapolis, Ind.) was added and incubated at 37°C for 30 min in a humidified atmosphere. After the cells were washed with PBS, affinity-purified biotinylated goat anti-rabbit IgG (Boehringer Mannheim) was added and incubated for 30 min at 37°C as before. The cells were washed with PBS, and avidin conjugated with fluorescein was added and incubated with the cells at 37°C for 30 min as before. Standard immunofluorescence was performed similarly with MAb 327, followed by biotinylated affinity-purified goat anti-mouse IgG and by avidin conjugated with fluorescein or with rabbit antiactin antibodies followed by biotinylated affinity-purified goat anti-rabbit IgG and then by avidin conjugated with fluorescein. The cover slips were washed with PBS, mounted in Elvanol, viewed with a 63× objective in a Zeiss Universal microscope equipped with epifluorescence illumination, and photographed on Tri-X Pan-film (Eastman Kodak Co., Rochester, N.Y.).

RESULTS

Retrovirus vector containing c-*src*-coding sequences lacks transforming activity. The c-*src*-coding sequence was stably introduced into MDCK cells by using helper-free, defective, amphotropic retroviruses (50). The retroviral vectors contain the neomycin resistance gene (Tn*5* Neo^r) and therefore enable selection of infected cells for resistance to the toxic aminoglycoside G418 (Fig. 1A). The pMc-*src*ΔiSVneo provirus construct contains the c-*src*-coding sequence controlled by the Moloney LTR promoter and has the Tn*5* Neo^r gene placed downstream from an internal simian virus 40 early region enhancer-promoter segment. The control vector, pFVXMneo, contains the Tn*5* Neo^r gene which is under the control of the Moloney LTR promoter.

Amphotropic viral stocks of Mc-*src*ΔiSVneo and FVXM neo were harvested from ψAM producer cells and compared

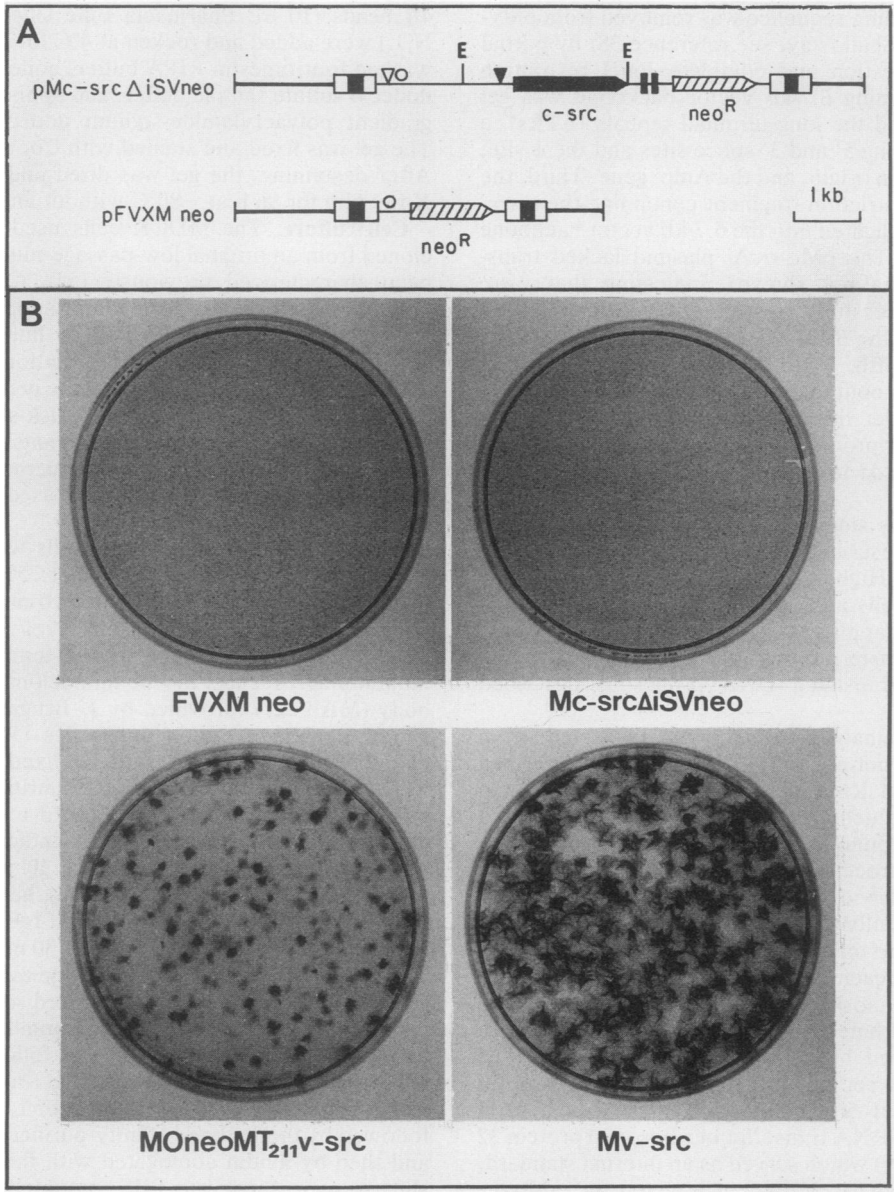

FIG. 1. (A) Retrovirus vector constructions. A schematic map of the provirus insert from each plasmid is shown. The plasmid designations are given on the left. pMc-*src*ΔiSVneo contains the c-*src*-coding sequence under control of the Moloney LTR promoter and an additional transcriptional unit composed of the Tn*5* aminoglycoside phosphotransferase (Tn*5* Neo^r)-coding region which is under the control of an internal simian virus 40 early region enhancer-promoter segment. The pFVXMneo provirus contains only the Tn*5* Neo^r gene under the control of the Moloney LTR promoter. Symbols: open boxes, LTR sequences; open circle, virus genome packaging signal (ψ); open arrowhead, 5′ splice site; solid arrowhead, 3′ splice site; solid rectangles, simian virus 40 early region enhancer-promoter segment; thick lines, rat genome DNA derived from original provirus clone; E, *Eco*RI restriction site. (B) Focus formation assay. One petri dish (100 mm) containing 5×10^5 rat-1 cells was infected with $\geq 10^5$ infectious virus particles (Neo^r units) of FVXMneo, Mc-*src*ΔiSVneo, or MOneoMT$_{211}$v-*src* amphotropic virus stock and selected for resistance to G418. A mixed population of Rat-1 cells derived by infection with each of these virus stocks was tested for focus-forming ability as described previously (72). A dish of Rat-1 cells which was infected with a high-pp60$^{v\text{-}src}$-expressing virus, Mv-*src*, and assayed for focus-forming ability is shown for comparison.

with viral stocks of MOneoMT$_{211}$v-*src* (a low-v-*src*-expressing virus [72]) and Mv-*src* (a high-v-*src*-expressing virus [72]) for their ability to transform rat-1 cells. The two v-*src*-expressing viruses, MOneoMT$_{211}$v-*src* and Mv-*src*, exhibited a low and high degree of focus-forming activity, respectively (Fig. 1B, lower panels). However, Mc-*src*ΔiSVneo lacked focus-forming activity, since G418^r Rat-1 cells derived by infection with Mc-*src*ΔiSVneo (Fig. 1B, upper right panel) were indistinguishable in this assay from G418^r rat-1 cells derived by infection with FVXMneo (Fig. 1B, upper left panel) or uninfected rat-1 cells (data not shown). In addition, the rat-1 cell populations derived by infection with the v-*src*-expressing viruses exhibited soft agar growth potential, but rat-1 cells derived by infection with Mc-*src*ΔiSVneo or FVXMneo failed to grow in agar suspension (data not shown). Finally, all MDCK cell clones derived by infection with Mc-*src*ΔiSVneo (see below) lacked anchorage-independent growth potential and focus-forming

potential (data not shown). These data demonstrate that Mc-*src*ΔiSVneo is not a transforming virus and that the viral stocks contain no detectable spontaneous transforming mutants.

MDCK epithelial cells expressing elevated levels of pp60$^{c\text{-}src}$. MDCK cells were infected with either Mc-*src*ΔiSVneo or FVXMneo virus and selected in G418. Five representative clones were picked and expanded for detailed analysis. The presence of a proviral insertion in the genome of each clone was demonstrated by Southern blot analysis. High-molecular-weight DNA from each clone was digested with *Eco*RI, electrophoresed through an agarose gel, transferred to nitrocellulose, and hybridized to a nick-translated SVneo probe (Fig. 2, lanes a to f). The provirus sequence contains an *Eco*RI site between the c-*src*-coding region and SVneo sequences (Fig. 1A). DNA from each clone had a different-sized band that hybridized to the SVneo probe, indicating that each cell clone has a single provirus insertion. A second *Eco*RI site exists in the intron, approximately 800 base pairs upstream from the ATG codon of c-*src*. Hybridization with a nick-translated c-*src* probe revealed the presence of a single band (~2.5 kb) in each clone containing the Mc-*src*ΔiSVneo provirus (Fig. 2, lanes g to l), indicating that no gross rearrangements or deletions were detectable within the c-*src*-coding region.

The level of c-*src* expression was determined by Northern blot analysis and by an in vitro pp60$^{c\text{-}src}$ kinase assay (Fig. 3). For each type of analysis, the MFN-2 control cells and cells of each clone were grown to approximately the same subconfluent cell density. Total RNA (25 μg) from each clone was electrophoresed through a formaldehyde-containing agarose gel, transferred to nitrocellulose paper, and hybridized to a nick-translated c-*src* probe (Fig. 3A). The resulting autoradiogram shows that each cell clone containing an Mc-*src*ΔSVneo provirus expressed elevated levels of two RNA species (~5.8 and ~4 kb) which hybridized to the c-*src* probe. Hybridization with a nick-translated SVneo probe identified the same pair of transcripts (data not shown), which presumably represent the genomic proviral transcript (unspliced) and the subgenomic proviral transcript (spliced), respectively. These two RNA species were absent in the MFN-2 cells (Fig. 3A, lane 2). The endogenous c-*src* RNA transcript in the MFN-2 control cells was detected after longer exposure of the autoradiograms and could be distinguished from the exogenous c-*src* RNA species by its slightly smaller size of ~3.9 kb (Fig. 3A, lane 1). The following relative levels of c-*src* RNA expression were determined quantitatively as described in the Materials and Methods: MFN-2, 1; Mc1, 8; Mc2, 8; Mc3, 11; Mc4, 8; and Mc5, 15.

The amount of pp60$^{c\text{-}src}$ enzyme expressed in each clone was determined by an in vitro kinase assay. Cell extracts

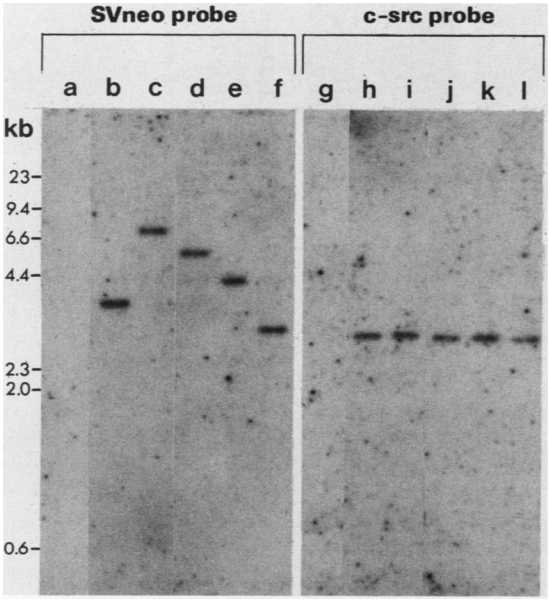

FIG. 2. Southern blot analysis of MDCK cell lines expressing elevated levels of pp60$^{c\text{-}src}$ and the control MFN-2 cells. High-molecular-weight DNA (13 μg) was digested with *Eco*RI, electrophoretically separated, transferred to nitrocellulose, and hybridized with either a ^{32}P-labeled nick-translated SVneo probe or an c-*src* probe. Lanes: a and g, MFN-2; b and h, Mc1; c and i, Mc2; d and j, Mc3; e and k, Mc4; f and l, Mc5. λ *Hin*dIII relative molecular size markers are given in kilobases (kb) on the left.

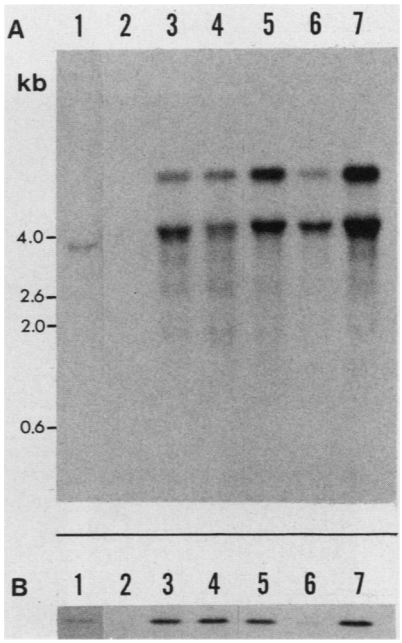

FIG. 3. (A) Northern blot analysis of MDCK cell lines expressing elevated levels of pp60$^{c\text{-}src}$ and control MFN-2 cells. Total RNA (25 μg) was denatured with formamide-formaldehyde and separated with a formaldehyde-containing 1% agarose gel, transferred to nitrocellulose, and hybridized with a ^{32}P-labeled, nick-translated c-*src* probe. Lanes: 1, MFN-2; 2, MFN-2; 3, Mc1; 4, Mc2; 5, Mc3; 6, Mc4; 7, Mc5. The autoradiogram of lane 1 was exposed for 24 h. The autoradiograms of lanes 2 to 7 were exposed for 1 h. Relative molecular mass markers are given in kilobases (kb) on the left-hand margin: 4.6 kb, spliced Mc-*src*ΔiSVneo transcript; 2.6 kb, β subunit of Na^+,K^+-ATPase mRNA (dog); 2.0 kb, actin mRNA (dog); 0.6 kb, ribosomal protein 32 (dog). (B) pp60$^{c\text{-}src}$ kinase assay of MDCK cell lines expressing elevated levels of pp60$^{c\text{-}src}$ and control MFN-2 cells. The protein kinase assay with [γ-^{32}P]ATP was performed on pp60$^{c\text{-}src}$ specific immunoprecipitates prepared from each MDCK cell line, normalized to total protein content. The immunoprecipitates were applied to a 7 to 15% linear gradient sodium dodecyl sulfate-polyacrylamide gel and electrophoresed. Portions of the resulting autoradiograms are presented and reveal specific ^{32}P labeling of the IgG heavy chains. Lanes: 1, MFN-2; 2, MFN-2; 3, Mc13.2; 4, Mc13.8; 5, Mc13.22; 6, Mc18.5; 7, Mc18.7. The autoradiogram of lane 1 was exposed for 51 h. The autoradiograms of lanes 2 to 7 were exposed for 17 h.

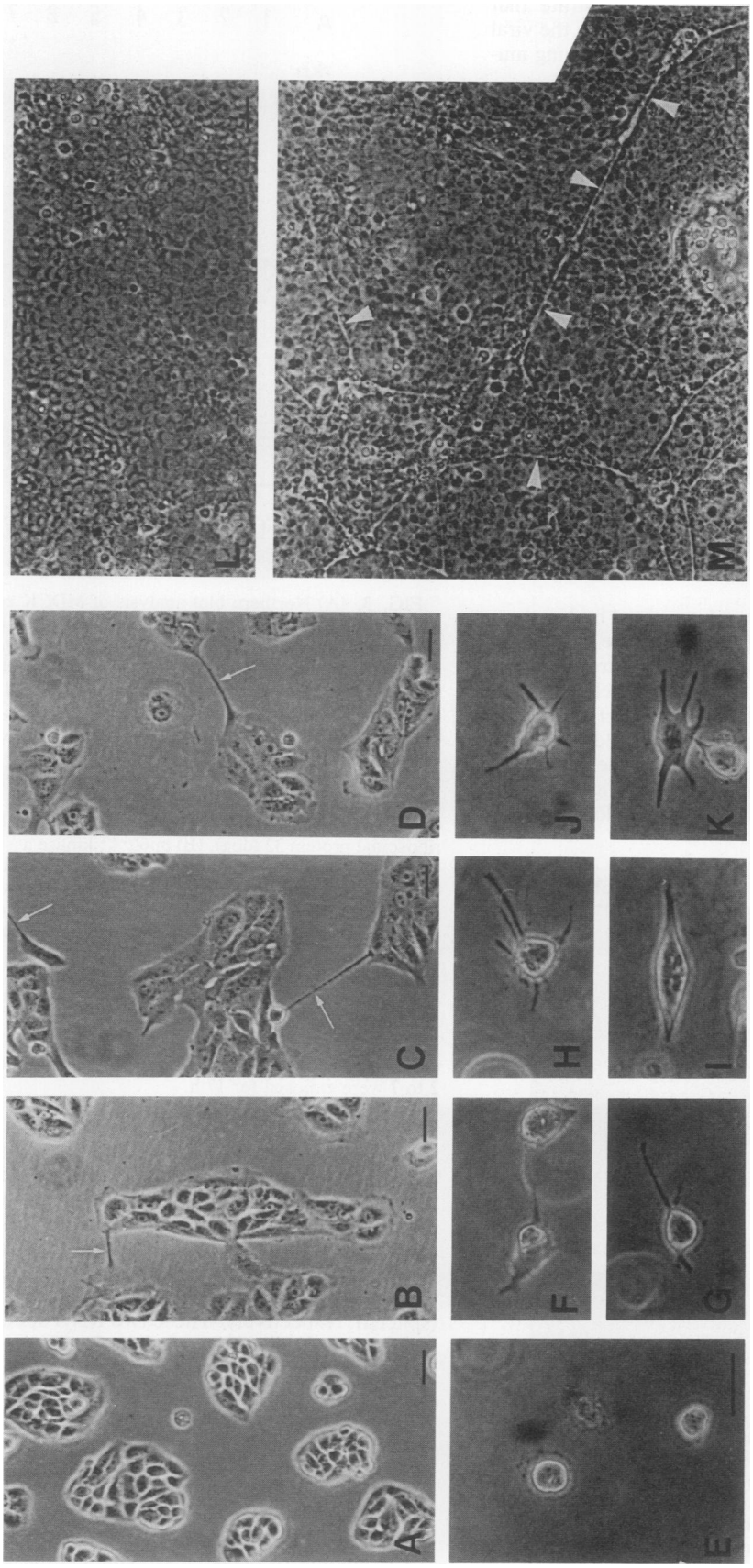

FIG. 4. Morphology of MDCK cells expressing elevated levels of $pp60^{c\text{-}src}$ and control MFN-2 cells. Cells were subcultured on plastic petri dishes at similar initial densities ($\sim 10^4/cm^2$) and photographed 3 days later with phase-contrast optics (A to D). Cells were seeded into collagen gel matrix as described previously (72) and photographed 1 day later (E to K). Cells were allowed to grow to confluency and then overlaid with 0.33% agar containing complete medium and photographed 7 days later (L and M). (A) MFN-2; (B) Mc4; (C) Mc3; (D) Mc5; (E) MFN-2; (F) Mc4; (G) Mc1; (H) Mc2; (I) Mc3; (J) Mc5; (K) Mc5; (L) MFN-2; (M) Mc5. Arrows show cell processes of MDCK cells expressing elevated levels of $pp60^{c\text{-}src}$ (B to D). Arrowheads show long processes formed by Mc5 cells (M). Bars, 15 μm.

were normalized to total protein and immunoprecipitated with a monoclonal antibody (MAb) raised against pp60$^{v\text{-}src}$ that recognizes pp60$^{c\text{-}src}$ (46). In vitro phosphorylation of IgG heavy chains was performed as described previously (13, 72). All clones had levels of pp60$^{c\text{-}src}$ kinase activity greater than that of the MFN-2 control cells (Fig. 3B). Longer exposures of autoradiograms were required to detect kinase activity in immunoprecipitates of MFN-2 cell extracts than in immunoprecipitates of the cells containing the Mc-*src*ΔiSVneo provirus (Fig. 3B, lane 1). For quantitation of relative kinase levels, the total pp60$^{c\text{-}src}$ kinase level of each clone was divided by the level of pp60$^{c\text{-}src}$ kinase activity of the MFN-2 control cells to give the following values: MFN-2, 1; Mc1, 3.2; Mc2, 3.3; Mc3, 3.4; Mc4, 1.1; and Mc5, 9.2. Thus, the relative pp60$^{c\text{-}src}$ kinase levels of the clones correlate roughly with the relative levels of c-*src* RNA expression determined by Northern blot analysis.

MDCK cells expressing elevated levels of pp60$^{c\text{-}src}$ exhibit marked changes in cell shape. At low density, MFN-2 control cells formed discrete colonies with smooth, rounded edges (Fig. 4A). The MDCK cell clones expressing elevated levels of pp60$^{c\text{-}src}$ also formed discrete colonies under these conditions, but all the cells were very flat and elongated and, at the edges of the colonies, bore prominent processes (Fig. 4B to D). However, at moderate cell densities ($\sim 2 \times 10^5/cm^2$), the cells of each clone became closely packed to form a continuous monolayer which closely resembled that formed by the parent MDCK cells (data not shown; for confluent control MFN-2 cells, see Fig. 4L).

A conspicuous feature of the MDCK cells expressing elevated levels of pp60$^{c\text{-}src}$ was their ability to form cell processes, which became even more apparent when the cells were grown to confluency. Two to three days after reaching confluency, many of the cells of each clone began to extend long, attenuated processes that burrowed beneath the monolayer for distances of up to 200 μm, which is approximately 20-fold greater than the dimensions of a control MDCK cell (~10 μm) (Fig. 4M). After a week of growth, the epithelial monolayer was partially undermined by an extensive meshwork of cell processes (Fig. 4M, arrowheads). An analysis of the processes by electron microscopy has confirmed the subepithelial location of the processes and indicates that the processes do not contain nuclei (unpublished data). Significantly, the level of pp60$^{c\text{-}src}$ expression correlated with the severity of change in cell shape; the highest-pp60$^{c\text{-}src}$-expressing MDCK cell clone, Mc5, formed processes earlier and formed a more extensive meshwork of processes than any other clone. The lowest-pp60$^{c\text{-}src}$-expressing clone, Mc4, exhibited the least extensive meshwork of processes (data not shown). Control MFN-2 cells did not exhibit this trait (Fig. 4L).

Elevated levels of pp60$^{c\text{-}src}$ alter the morphogenesis of polarized, multicellular (MDCK) cysts. The fact that elevated expression of pp60$^{c\text{-}src}$ markedly alters the morphological properties of individual MDCK cells prompted us to determine whether these cells still retained the morphogenetic properties necessary to form tissuelike, multicellular epithelial cysts in a collagen gel matrix in vitro (72). Under these conditions, normal MDCK cells divide clonally to form a spherical cyst composed of a closed monolayer of polarized cells in which the apical membranes face the lumen of the cyst and the basal membranes form a smooth, outer surface exposed to the collagen gel matrix (Fig. 5A and B; see also Fig. 6A).

One day after seeding the cells in the collagen gel matrix, it was noted that, without exception, all the MFN-2 control cells exhibited a rounded shape without visible cell processes (Fig. 4E). However, approximately 25 to 75% of the cells from each of the high-pp60$^{c\text{-}src}$-expressing MDCK cell clones exhibited a dramatic change in cell shape. Some cells exhibited a bipolar, spindle shape (Fig. 4I), but more frequently they assumed bizarre stellate shapes, with multiple processes extending from the cell body (Fig. 4F, G, H, J, and K). Only a fraction of the cells from each high-pp60$^{c\text{-}src}$-expressing cell clone exhibited altered shapes in the collagen gel matrix, even though 100% of the cells exhibited a distorted cell shape when plated on a two-dimensional substratum (Fig. 4B to D); this may reflect differences between the two-dimensional plastic substratum and the three-dimensional collagen gel substratum. The three-dimensional substratum, which exhibits random variations in the consistency of the collagen gel, presumably provides a less uniform surface for cell attachment than the two-dimensional plastic substratum. This explanation is supported by the fact that the shape of the high-pp60$^{c\text{-}src}$-expressing MDCK cells can be distorted in a predictable manner by gently stretching the collagen gel matrix surrounding the cells with sterile forceps (unpublished data). Within a few hours after this manipulation, cells in the vicinity of the applied tension exhibited a bipolar shape with cell processes oriented parallel to the direction of the applied force. The same manipulation did not alter the cell shape of control MDCK cells (data not shown).

Six days after seeding, the high-pp60$^{c\text{-}src}$-expressing MDCK cells formed cysts with deformed architecture (Fig. 5). Whereas 100% of the MFN-2-derived cysts were spherical, over 90% of the cysts formed by each of the high-pp60$^{c\text{-}src}$-expressing clones exhibited irregular, nonspherical shapes (Fig. 5C to H). Some cysts formed by the high-pp60$^{c\text{-}src}$-expressing cells were spherical over part of their surface, but contained a few bleblike protrusions (Fig. 5C and F); other cysts were markedly distorted with an elongated conformation (Fig. 5E, G, and H). Significantly, these irregularly shaped cysts were composed of intact epithelial monolayers that exhibited no apparent disruption of the two-dimensional relationship between the cells. Although occasional cell processes extended from the basal aspect of some cysts into the collagen gel matrix, entire cells were not displaced from the epithelial monolayer into the surrounding collagen gel matrix.

These results indicate that elevated levels of pp60$^{c\text{-}src}$ confer on MDCK cell monolayers the ability to form structures with multiple three-dimensional shapes, whereas control MDCK cells form only spherical structures. Apparently, these cysts are able to maintain the two-dimensional relationships among the cells that form the monolayer, but are unable to maintain the rigid, spherical three-dimensional architecture exhibited by control cysts. These observations suggested to us that the morphogenesis of multicellular epithelial cysts composed of high-pp60$^{c\text{-}src}$-expressing MDCK cells was highly susceptible to distortion by physical constraints of the surrounding collagen gel matrix. To test this possibility, we assayed the morphogenetic properties of MFN-2 cells and high-pp60$^{c\text{-}src}$-expressing MDCK cells under conditions that led to a predictable distortion of the three-dimensional conformation of all cysts. In this assay, MDCK cell cysts were grown in the interface between two layers of collagen gel matrix, a condition that causes normal MDCK cells to form biconvex, disk-shaped cysts rather than spherical cysts (see diagram in Fig. 5I; also see reference 72). The MFN-2 cells formed cysts indistinguishable from those of parent MDCK cells that maintained relatively large,

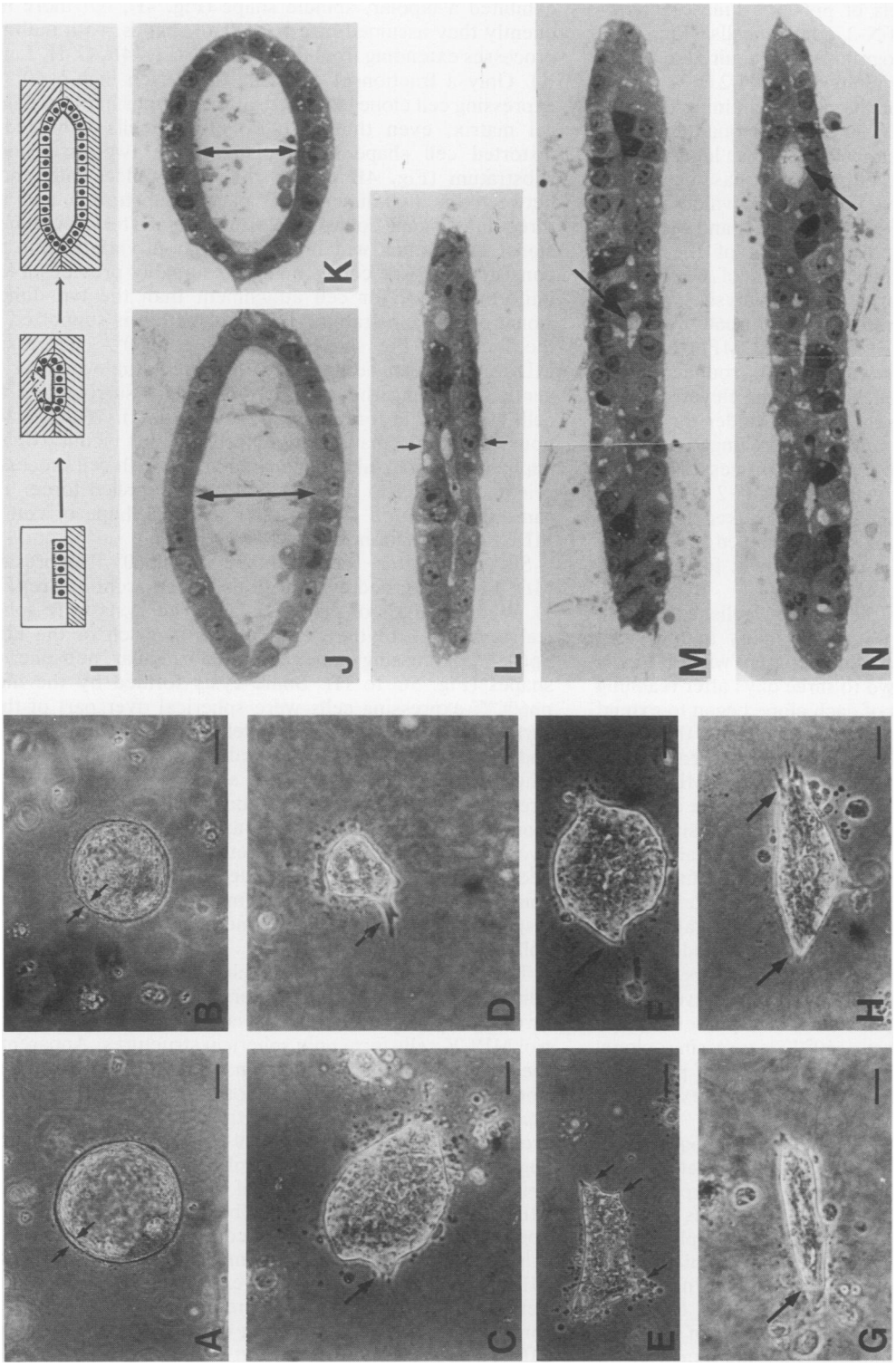

FIG. 5. Formation of multicellular (MDCK) cysts grown in a collagen gel matrix. Control MFN-2 cells and MDCK cells expressing elevated levels of $pp60^{c\text{-}src}$ were seeded directly into a three-dimensional collagen gel matrix and allowed to grow for 6 days (A to H). To form disk-shaped, multicellular (MDCK) cysts (J to N), the cells were grown on a flat two-dimensional collagen gel substratum and then overlaid with a second layer of collagen gel matrix as illustrated diagramatically in panel I. The cysts on the left were photographed on day 6 with phase-contrast optics (A to H). The cysts on the right were fixed and embedded as described previously (72), and thin sections (3 μm) were prepared (J to N). The sections were stained with toluidine blue and photographed on day 6 with bright-field optics (J to N). (A and B) MFN-2 (control); (C) Mc5; (D) Mc3; (E) Mc5; (F) Mc5; (G) Mc3; (H) Mc4; (J) MFN-2; (K) MFN-2; (L) Mc5; (M) Mc5; (N) Mc5. Arrows in panels A and B show the profile of the epithelial monolayer in focus. Arrows in panels C to H show cell processes projecting from the basal aspect of the cyst wall into the collagen gel matrix. Double arrows in panels J and K show wide, open lumens formed by control MFN-2 cells. Small arrows in panel L show flat morphology of the Mc5 cysts which exhibit a slitlike lumen. Arrows in panels M and N show patent areas of the lumen. Bars in panels A to H, 20 μm. Bars in panels J to N, 10 μm.

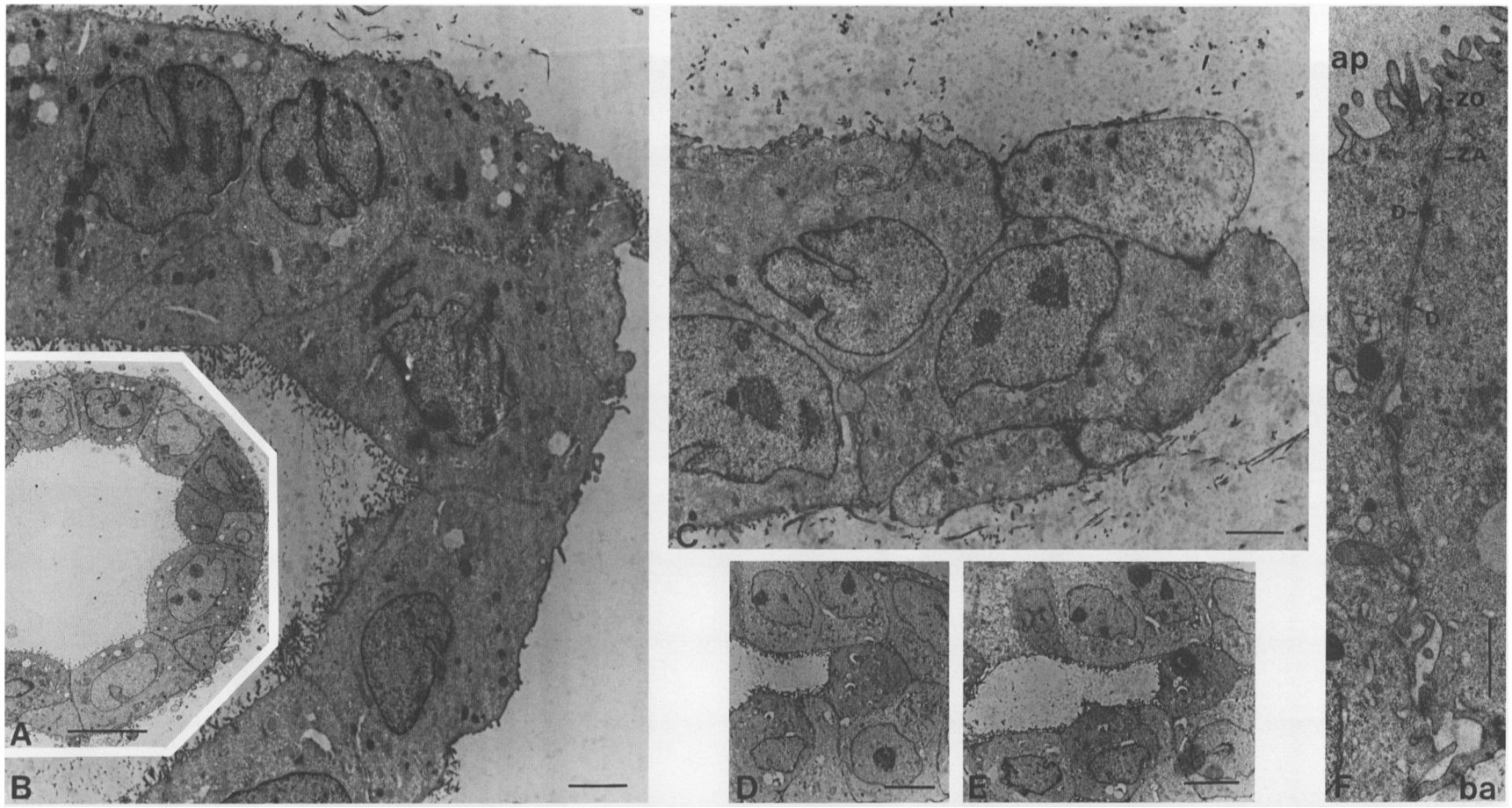

FIG. 6. Ultrastructure of multicellular cysts composed of MFN-2 (control) cells and MDCK cells expressing elevated levels of pp60$^{c\text{-}src}$. MDCK cells were cultured in a three-dimensional collagen gel matrix for 6 days and then processed for analysis by transmission electron microscopy (A to E). The cells in panel F were grown on a planar, two-dimensional collagen gel substratum and processed similarly. (A) Low-power electron micrograph showing section of spherical multicellular cyst composed of MFN-2 (control) cells. (B) Low-power electron micrograph showing edge of a disk-shaped cyst composed of MFN-2 (control) cells. (C) Low-power electron micrograph showing edge of a flat cyst composed of MDCK cells which express elevated levels of pp60$^{c\text{-}src}$. (D and E) Low-power views of the discontinuous luminal spaces formed by high-pp60$^{c\text{-}src}$-expressing MDCK cells. (F) High-power electron micrograph showing area of cell-cell contact between two MDCK cells which express elevated levels of pp60$^{c\text{-}src}$. ap, Apical plasma membrane; ba, basal plasma membrane; zo, zonula occludens; D, desmosomes. Bars: 10 μm (A); 2.5 μm (B and C); 5 μm (D and E); 1 μm (F).

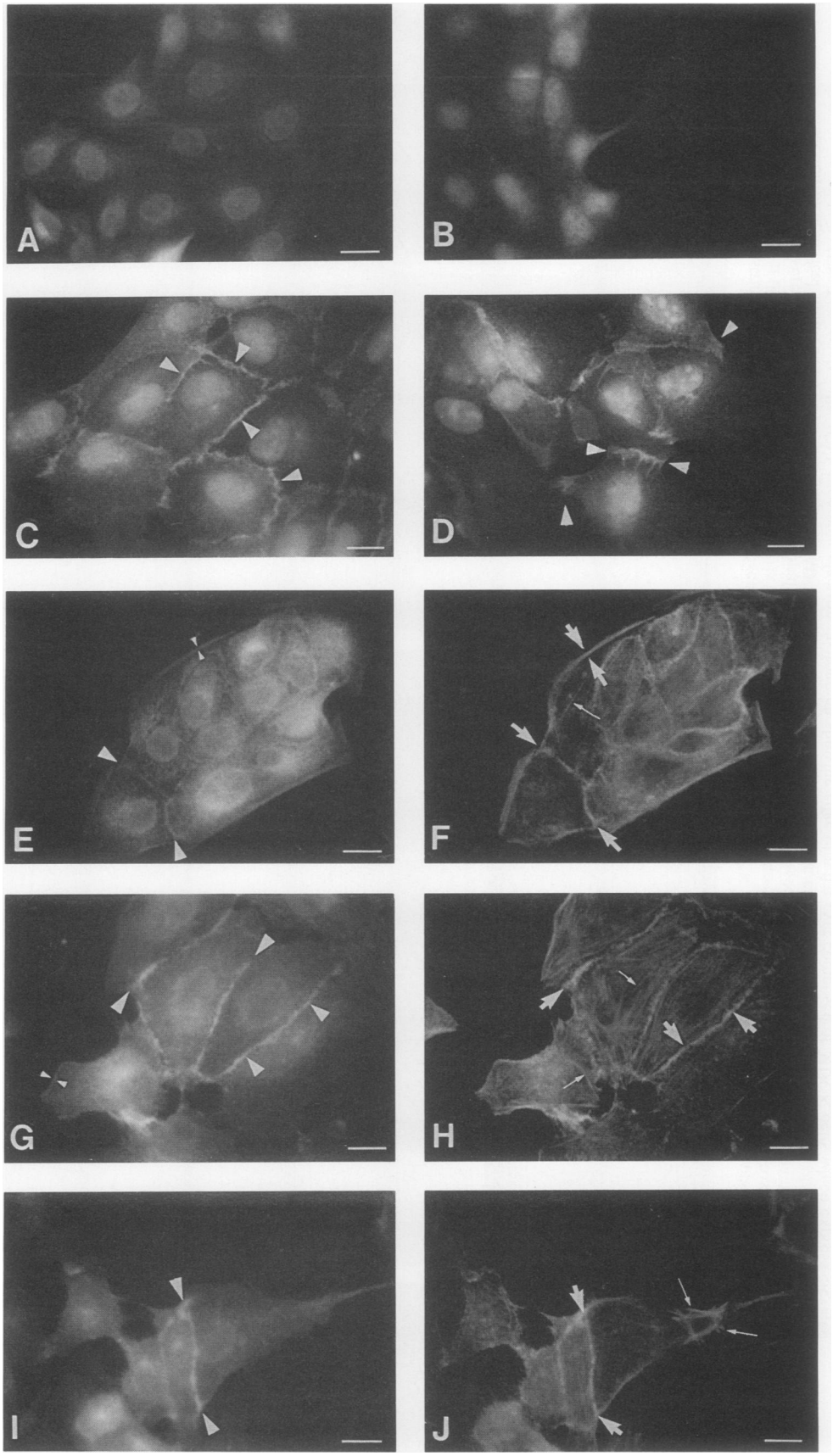
A
B
C
D
E
F
G
H
I
J

open lumens which were oval in cross section (Fig. 5J and K). However, the MDCK cells expressing elevated levels of pp60$^{c\text{-}src}$ formed completely flattened cysts under these conditions (Fig. 5L to N). At the resolution of the light microscope, an intact epithelial monolayer appeared to enclose a narrow, slitlike lumen in the cysts. These results demonstrated that elevated levels of pp60$^{c\text{-}src}$ regulate the morphogenetic properties which determine the shape of both single MDCK cells and multicellular epithelial structures composed of MDCK cells.

MDCK cells expressing elevated levels of pp60$^{c\text{-}src}$ exhibit distorted shapes but retain the ability to form morphologically normal cell-cell contacts. A low-power electron micrograph of a section through a spherical multicellular MFN-2 cell cyst showed that the epithelial monolayer was composed of cells that exhibited fairly uniform, semipyramidal shapes with the apical membrane oriented toward the lumen (Fig. 6A). An electron micrograph of a section through the edge of a disk-shaped MFN-2 cell cyst revealed that, in the region of the cyst wall which bends acutely, the shape of the individual cells is slightly distorted and less uniform than the shape of the MFN-2 cells in spherical cyst walls, but the cells still form a highly organized epithelial monolayer that maintains a curved contour at the edge of the cyst wall (Fig. 6B). In contrast, Mc5 cells grown under these conditions formed multicellular structures composed of epithelial monolayers that were folded at the edges in acute angles, which placed the cells of the superior and inferior aspects of the cyst walls into very close proximity (Fig. 6C). In fact, there were multiple cell-cell contacts, characterized by close apposition of cell membranes and occasional desmosomes, formed between cells in the superior aspect and cells in the inferior aspect of the cysts. In these regions, the cyst lumen appeared to be irregular and discontinuous in each plane of section (Fig. 6D and E; also see arrows in Fig. 5M and N). Significantly, the shape of the individual cells within the cyst wall was more distorted than that of the MFN-2 control cells, but these cells exhibited a high degree of cell-cell contact and established morphological polarity as indicated by the formation of a cyst lumen.

The ability of these cells to form morphologically normal cell-cell contacts was revealed more clearly by sectioning open epithelial monolayers grown on a planar, two-dimensional collagen gel matrix and analyzing them by transmission electron microscopy (Fig. 6F). A representative section through adjacent Mc5 cells showed a high degree of cell-cell contact between the membranes, which are closely apposed with rare instances of intercellular spaces greater than 50 nm (Fig. 6F). The Mc5 cells were morphologically polarized, exhibiting numerous apical microvilli and a well-developed apical junctional complex. The zonula occludens, located at the boundary of the apical and lateral membranes of the cell, was characterized by the very close opposition of adjacent cell membranes. The zonula adherens, characterized by an intercellular gap of ~20 nm, was present below the zonula occludens as demonstrated previously in normal MDCK cells (18, 63, 72). Finally, desmosomes with associated tonofilament bundles were located randomly on the lateral membranes. All high-pp60$^{c\text{-}src}$-expressing MDCK cell clones exhibited these ultrastructural features, which are indistinguishable from those exhibited by control MDCK cells (data not shown; see reference 72).

Areas of MDCK cell-cell contact are enriched with pp60$^{c\text{-}src}$. The fact that pp60$^{c\text{-}src}$ elicits an altered shape in highly differentiated epithelial cells prompted us to ask whether the distribution of pp60$^{c\text{-}src}$ immunoreactivity coincides with that of specific membrane-associated actin-containing structures inside the cell which have been implicated in the control of epithelial cell shape (see Discussion). Immunofluorescence microscopy was performed on MFN-2 control cells and all the MDCK cell clones expressing elevated levels of pp60$^{c\text{-}src}$, using an MAb raised against pp60$^{v\text{-}src}$ (MAb 237), a rabbit antiserum raised against canine actin, or both antibodies for double immunofluorescence (Fig. 7).

MFN-2 cells incubated with MAb 327 exhibited weak, but discrete linear staining of the cell periphery in regions of cell-cell contact and to a lesser degree on the free edge of cells (Fig. 7E). In addition, there was faint, diffuse pp60$^{c\text{-}src}$ staining that was more intense than the staining obtained with a nonimmune serum (compare Fig. 7A and E). All clones of high-pp60$^{c\text{-}src}$-expressing MDCK cells exhibited a staining pattern that was qualitatively similar to that of the MFN-2 cells, but discrete pp60$^{c\text{-}src}$ immunoreactivity was more intense in areas of cell-cell contact, and there was more intense, homogeneous pp60$^{c\text{-}src}$ immunoreactivity throughout the cells (Fig. 7C, D, G, and I).

MFN-2 cells incubated with antiactin antiserum exhibited discrete staining of actin filaments in three subcellular locations (Fig. 7F). First, there were multiple discrete spots in the apical plane of focus which corresponded to microvilli (data not shown). Second, there were linear striations in the basal plane of focus which represented stress fibers that have been shown to be associated at their ends with focal adhesion plaques on the plasma membrane (Fig. 7F, thin arrow; see references 23, 24, 32, and 74). Third, continuous linear staining was present in areas of cell-cell contact and on the free edge of the cells (Fig. 7F, thick arrows). MDCK cells expressing elevated levels of pp60$^{c\text{-}src}$ showed a similar pattern of actin immunofluorescence, except that the continuous line of immunoreactive actin which characterized the free edge of MFN-2 control cells appeared to be reorganized in the high-pp60$^{c\text{-}src}$-expressing cells; the free edge of many cells exhibited prominent stress fibers organized in a radiating pattern that coincided with lamellopodia and cell processes visualized by phase-contrast microscopy (Fig. 7H and J). Double immunofluorescence of MFN-2 control and high-pp60$^{c\text{-}src}$-expressing cells showed that the pattern of focal pp60$^{c\text{-}src}$ staining (Fig. 7E, G, and I, thick arrows) coincided

FIG. 7. Indirect immunofluorescence of MDCK cells expressing elevated levels of pp60$^{c\text{-}src}$ and control MFN-2 cells. Indirect immunofluorescence assays were performed on MDCK cells that had been fixed with 1.75% formaldehyde and permeabilized with 0.5% (vol/vol) Triton X-100 in PBS. The first antibody was nonimmune mouse IgG (A), a nonimmune rabbit serum (B), a MAb directed against pp60$^{v\text{-}src}$ (C, D, E, G, I), or rabbit antiactin polyclonal antibody (F, H, and J). The second antibody was biotinylated goat anti-mouse IgG (A, C, and D) or a combination of rhodamine-conjugated goat anti-mouse IgG and biotinylated goat anti-rabbit IgG (B, E to J). The third reagent was fluorescein-conjugated avidin (A to J). (A) Mc5; (B) Mc5; (C) Mc1; (D) Mc4; (E and F) MFN-2; (G and H) Mc2; (I and J) Mc5. Large arrowheads show pp60$^{c\text{-}src}$ immunoreactivity in areas of cell-cell contact (C, D, E, G, I). Small arrowheads show pp60$^{c\text{-}src}$ immunoreactivity on the free edge of the cells (E and G). Thick arrows show actin immunoreactivity in areas of cell-cell contact (F, H, and J). Thin arrows show actin stress fibers (F, H, and J). Nuclear immunofluorescence is exhibited by cells incubated with control antibody (A and B) and with anti-pp60^{src} antibody (C, D, E, G, I) and is therefore considered nonspecific immunoreactivity. All photographs are presented at the same exposure and the same magnification. Bars, 5 μm.

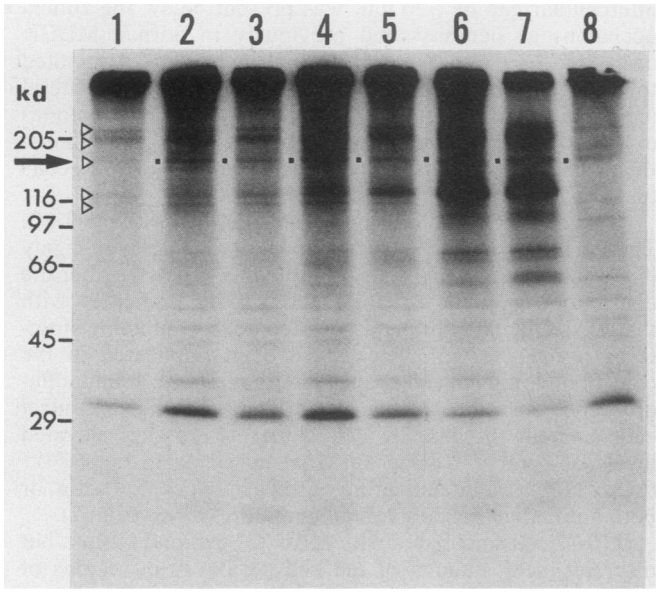

FIG. 8. Phosphotyrosine-containing phosphoproteins immunoprecipitated from control MFN-2 cells, MDCK cells expressing elevated levels of pp60$^{c\text{-}src}$, and MDCK cells expressing pp60$^{v\text{-}src}$. Cells were labeled metabolically with $^{32}P_i$ for 15 h and extracted with RIPA buffer. Samples were normalized to total protein content and immunoprecipitated with a polyclonal rabbit antibody directed against phosphotyrosine (17). Immunoprecipitates were separated by 5 to 15% sodium dodecyl sulfate-polyacrylamide gel electrophoresis, dried, and exposed to X-ray film for 5 h. The resulting autoradiogram is presented. Lanes: 1, MFN-2; 2, Mc4; 3, Mc5; 4, MMTv-10 (low-pp60$^{v\text{-}src}$-expressing MDCK cell line); 5, MMTv-7 (low-pp60$^{v\text{-}src}$-expressing MDCK cell line); 6, MMTv-60 (MDCK cell line transformed by pp60$^{v\text{-}src}$); 7, Mv-*src*-9 (high-pp60$^{v\text{-}src}$-expressing cell line); 8, control (Mv-*src*-9 cell extract immunoprecipitated with nonimmune rabbit serum). Relative molecular mass markers are indicated in kilodaltons (kd): 25 kDa, myosin heavy chain; 116 kDa, β-galactosidase; 97.5 kDa, phosphorylase *b*; 68 kDa, bovine serum albumin; 45 kDa, ovalbumin; 29.5 kDa, carbonic anhydrase. Arrowheads on left-hand margin show R_f values corresponding to molecular masses of 210, 190, 160, 120, and 110 kDa. The arrow on the left-hand margin and the dots between the lanes mark the R_f value corresponding to the ~160-kDa protein species.

with the pattern of immunoreactive actin only in areas of cell-cell contact (Fig. 7F, H, and J, arrowheads). Little or no focal pp60$^{c\text{-}src}$ immunofluorescence was detected on the basal aspect of the cells which exhibited subcortical actin-containing stress fibers (compare Fig. 7I and J).

MDCK cells expressing elevated levels of pp60$^{c\text{-}src}$ exhibit increased phosphorylation of a more limited number of phosphotyrosine-containing proteins than MDCK cells expressing pp60$^{v\text{-}src}$. We analyzed the level of phosphorylation of phosphotyrosine-containing proteins in control MDCK cells, high pp60$^{c\text{-}src}$-expressing MDCK cells, and pp60$^{v\text{-}src}$-expressing MDCK cells to compare the phenotypes of these cells at a biochemical level. A polyclonal antiphosphotyrosine antibody (17) was used to immunoprecipitate phosphotyrosine-containing proteins from cell extracts of MFN-2 cells, Mc4 cells, Mc5 cells, and four MDCK cell lines expressing different levels of pp60$^{v\text{-}src}$ which had been labeled with $^{32}P_i$ for 15 h (Fig. 8). All MDCK cell lines, including the MFN-2 control cells, exhibited multiple bands corresponding to phosphotyrosine-containing proteins. However, for comparative purposes, we concentrated in this analysis on seven prominent phosphotyrosine-containing proteins with apparent molecular sizes of ~220, ~190, ~160, ~120, ~110, ~80, and ~60 kilodaltons (kDa) (Fig. 8, indicated by arrowheads at left margin of autoradiogram). The ~220-, ~190-, ~120-, and ~110-kDa bands are similar in intensity in the MFN-2 control cells and the MDCK cells expressing elevated levels of pp60$^{c\text{-}src}$ (Fig. 8, lanes 1 to 3). However, the relative intensity of the ~160-kDa band compared with the ~220-, ~190-, ~120-, and ~110-kDa bands is higher in MDCK cell lines expressing elevated levels of pp60$^{c\text{-}src}$ than in MFN-2 cells (Fig. 8, lanes 2 and 3). In contrast, MDCK cell lines expressing low levels of pp60$^{v\text{-}src}$ showed increased phosphorylation of the ~220-, ~190-, ~160-, ~120-, and ~110-kDa proteins compared with the MFN-2 cells and high-pp60$^{c\text{-}src}$-expressing MDCK cells (Fig. 8, lanes 4 and 5). The MDCK cell lines transformed by elevated levels of pp60$^{v\text{-}src}$ exhibited more intense bands corresponding to the ~190-, ~160-, and ~120-kDa phosphoprotein species, in addition to prominent bands corresponding to phosphoproteins with molecular weights of ~80 and ~60 kDa (Fig. 8, lanes 6 and 7). Finally, it is evident that in all pp60$^{v\text{-}src}$-expressing MDCK cell lines, the two bands corresponding to phosphoproteins of ~190 and ~120 kDa are more intense than the band corresponding to the ~160-kDa phosphoprotein species (Fig. 8, lanes 4 to 7). In conclusion, these data show that of the seven phosphotyrosine-containing proteins compared in this analysis, only one exhibited increased phosphorylation in MDCK cells expressing elevated levels of pp60$^{c\text{-}src}$, whereas multiple proteins exhibited increased phosphorylation in MDCK cells expressing pp60$^{v\text{-}src}$.

DISCUSSION

Detection of a nonmitogenic biological action of pp60$^{c\text{-}src}$ by the MDCK cell assay. MDCK cells are able to generate multicellular epithelial structures in vitro which show a striking structural and functional resemblance to epithelial tissue structures in vivo (10, 11, 30, 52, 59, 70). The formation of these multicellular structures depends on morphogenetic determinants that control the degree of adhesion between MDCK cells and those which establish and maintain the fixed cuboidal shape of MDCK cells (72; also see below). MDCK cells are already highly differentiated and do not undergo a sequential inductive process to form multicellular structures, which characterizes epithelial morphogenesis in situ (3, 28). For this reason, the alteration of the morphogenetic properties of MDCK cells may be attributed to the elevated expression of an introduced gene and not to independent inductive factors.

Using these properties of MDCK cells, we found that pp60$^{c\text{-}src}$ induces a nonmitogenic, pleomorphic phenotype which manifests itself as a predictable change in the shape of highly differentiated epithelial cells and multicellular epithelial structures in vitro. In contrast, fibroblasts expressing elevated levels of pp60$^{c\text{-}src}$ were morphologically indistinguishable from control fibroblasts (data not shown; see Fig. 1B and reference 56). The reason for this difference may be that the biological action of pp60$^{c\text{-}src}$ manifests itself less overtly in fibroblasts than in MDCK cells, because normal fibroblasts are already able to form prominent cell processes and do not form highly organized tissuelike multicellular structures in vitro. Thus, MDCK cells provide a sensitive biological assay to study the nonmitogenic action(s) of the pp60$^{c\text{-}src}$ tyrosine kinase.

pp60$^{c\text{-}src}$ exhibits a more discriminatory biological action than pp60$^{v\text{-}src}$. Our previous study showed that low-level expression of pp60$^{v\text{-}src}$ in MDCK cells did not have a

mitogenic effect, but led to a flat, spread-out cells (including the formation of cell processes) and a disturbance of selective epithelial cell-cell adhesion components (72). The present studies demonstrated that MDCK cells expressing elevated levels of pp60$^{c\text{-}src}$ exhibit marked alterations of cell shape (pleomorphism), but in contrast to MDCK cells expressing pp60$^{v\text{-}src}$, these cells from morphologically normal cell-cell contacts. Three facts indicate that the MDCK cells expressing elevated levels of pp60$^{c\text{-}src}$ exhibit a high degree of cell-cell adhesion, a property which correlates with the high degree of cell-cell contact observed by electron microscopy. First, whole cells were not displaced from the basal aspect of multicellular epithelial cysts into the surrounding collagen gel matrix, as was demonstrated previously for MDCK cells expressing low levels of pp60$^{v\text{-}src}$ (Fig. 5 and 6) (72). Second, cells were not displaced (shed) from the apical aspect of confluent epithelial monolayers grown in petri dishes and overlaid with agar-containing medium, as demonstrated previously for MDCK cells expressing low levels of pp60$^{v\text{-}src}$ (Fig. 4M) (72). Third, these cells express steady-state levels of a canine epithelial cell adhesion molecule, rr-1 (29), that are similar or identical to that expressed by control MDCK cells (unpublished data). Thus, elevated levels of pp60$^{c\text{-}src}$ induced in MDCK cells a subset of the phenotypic traits which were induced by low levels of pp60$^{v\text{-}src}$; MDCK cells expressing elevated levels of pp60$^{c\text{-}src}$ exhibit changes in the shape of single cells and multicellular structures, but they show neither a disturbance of cell-cell contact nor a loss of growth control.

These qualitative biological differences between the phenotypes induced by pp60$^{c\text{-}src}$ and pp60$^{v\text{-}src}$ could theoretically be due to differences in the biochemical specificity of these enzymes. Our comparison of phosphotyrosine-containing proteins in control MDCK cells, MDCK cells expressing elevated levels of pp60$^{c\text{-}src}$, and MDCK cells expressing pp60$^{v\text{-}src}$ demonstrated differences in phosphate incorporation into the seven phosphotyrosine-containing protein species considered in this analysis. We found that pp60$^{v\text{-}src}$ expression in MDCK cells led to increased phosphate incorporation into multiple phosphotyrosine-containing phosphoproteins with molecular sizes of ~220, ~190, ~160, ~120, ~110, ~80, and ~60 kDa compared with that in control MDCK cells. In contrast, of these seven phosphoproteins, only the ~160-kDa protein exhibited increased phosphorylation in high-pp60$^{c\text{-}src}$-expressing MDCK cells compared with that in MFN-2 control cells. We do not know whether the ~160-kDa phosphoprotein is phosphorylated on a tyrosine residue or whether it is a direct substrate for pp60$^{c\text{-}src}$, but these problems are being investigated. Nevertheless, the morphological and biochemical data taken together imply that in MDCK cells pp60$^{c\text{-}src}$ exhibits a more discriminatory biological action than pp60$^{v\text{-}src}$, because elevated pp60$^{c\text{-}src}$ expression leads to increased phosphorylation of a more limited set of protein(s) than does pp60$^{v\text{-}src}$.

How does pp60$^{c\text{-}src}$ induce a pleomorphic phenotype in MDCK cells? Our results showed that individual MDCK cells expressing elevated levels of pp60$^{c\text{-}src}$ exhibit a pleomorphic shape unlike the characteristic rounded shape of control MDCK cells cultured under identical conditions (Fig. 4E to K); furthermore, the shape of high-pp60$^{c\text{-}src}$-expressing MDCK cells, but not that of control MDCK cells, can be distorted by externally applied forces. In a three-dimensional collagen gel, multicellular cysts generated by high-pp60$^{c\text{-}src}$-expressing MDCK cells are also pleomorphic and are unable to maintain the characteristic spherical shape of cysts formed by control MDCK cells (Fig. 5A to H). When pp60$^{c\text{-}src}$-expressing MDCK cells were grown between two layers of collagen, the resulting multicellular cysts were deformed uniformly into a flat configuration with a slitlike lumen (Fig. 5L to N). In contrast, parent MDCK cells and MFN-2 control cells, which express low levels of pp60$^{c\text{-}src}$, were able to generate multicellular cysts that developed sufficient rigidity to expand the interface between the upper and lower layers of collagen gel matrix and to form a biconvex, disk-shaped structure with a large open lumen (Fig. 5J and K). These observations on the morphogenesis of multicellular MDCK epithelial structures in vitro indicate that elevated levels of pp60$^{c\text{-}src}$ allow the three-dimensional architecture of these cysts to adapt to the physical restrictions of the surrounding collagen gel matrix (i.e., the narrow interface between collagen layers). High-pp60$^{c\text{-}src}$-expressing MDCK cells apparently cannot develop multicellular structures with enough rigidity to expand the interface between the layers of collagen gel.

Taken together with the observation that MDCK cells expressing elevated levels of pp60$^{c\text{-}src}$ undergo marked changes of cell shape (e.g., the formation of long cell processes), these results indicate that the cell membrane is morphologically more plastic than that of control MDCK cells, which express low levels of pp60$^{c\text{-}src}$. It is possible that elevated levels of pp60$^{c\text{-}src}$ alter the ability of MDCK cell cysts to vectorially transport fluids and solutes, which could alter indirectly the rigidity and structure of the cysts. However, the ability of MDCK cells to form a physiologically competent, ion-pumping multicellular epithelium is not a necessary condition for detecting the nonmitogenic action of pp60$^{c\text{-}src}$, since the pp60$^{c\text{-}src}$-induced trait manifests as structural plasticity in single MDCK cells (Fig. 4). This indicates a direct effect of pp60$^{c\text{-}src}$ on the morphogenetic properties of MDCK cells. The fact that pp60$^{c\text{-}src}$ selectively alters this morphogenetic property of MDCK cells suggests strongly that pp60$^{c\text{-}src}$ acts on the elements within the cell which control the structural plasticity of the plasma membrane, without directly affecting the transduction of mitogenic signals or the function of specific epithelial cell adhesion structures.

Previous studies have shown that the shape and structural plasticity of animal cell membranes depend to a large extent on complex submembranous protein structures which contain actin filaments and multiple actin-binding proteins (51, 68, 73, 75). The shape of many types of epithelial cells is thought to be determined in part by actin-containing microfilaments, which are associated with the cytoplasmic aspect of the plasma membrane in areas of cell-cell contact (8, 39, 40, 53, 58, 65, 68, 75). Our analysis of the spatial distribution of pp60$^{c\text{-}src}$ in MDCK cells demonstrated that focal pp60$^{c\text{-}src}$ immunoreactivity coincides with focal actin immunoreactivity in regions of MDCK cell-cell contact. This suggests that pp60$^{c\text{-}src}$ could achieve a selective morphoregulatory effect on cell shape, at least in part, by altering the structural or mechanical properties of the actin-containing membrane skeleton in areas of cell-cell contact. In addition, the presence of increased homogeneous pp60$^{c\text{-}src}$ immunoreactivity throughout these flat MDCK cells suggests that pp60$^{c\text{-}src}$ acts on membrane-associated targets which are not in areas of cell-cell contact and which do not exhibit focal pp60$^{c\text{-}src}$ immunoreactivity, particularly since the most marked changes in cell membrane shape and in the pattern of actin immunoreactivity were observed in the free edges of these cells (e.g., cell processes and areas of extensive cell spreading). Although we do not know the molecular substrate(s) of pp60$^{c\text{-}src}$ in the MDCK cells, the data show that pp60$^{c\text{-}src}$ has

a biological activity and subcellular localization necessary to function as a selective regulator of the structural or mechanical properties of the plasma membrane-associated cytoskeleton.

In vivo implications of morphoregulatory action of pp60$^{c\text{-}src}$ on MDCK cells. The trait induced by pp60$^{c\text{-}src}$ in this in vitro system appears to resemble morphogenetic phenomena which characterize developing epithelial tissues in vivo. The formation of epithelial evaginations and more complex glandlike structures is thought to require spatial variations in the plasticity of the epithelium to give rise to movements that cause the monolayer to fold (33, 39, 65, 68, 75). The cells in folding regions of an epithelium exhibit shapes different from those of cells in flat regions of an epithelium (75). Movements of this type are thought to be regulated by a mechanism that modulates the degree of structural plasticity and shape of the cells, without disturbing the specific epithelial cell-cell contacts which are necessary to maintain the intact, two-dimensional organization of the epithelial monolayer (39, 65, 68, 75). We showed that elevated levels of pp60$^{c\text{-}src}$ can induce structural plasticity and an altered three-dimensional conformation of multicellular structures composed of MDCK cells without disturbing their ability to establish morphological polarity or their ability to form specific, adhesive cell-cell contacts which are necessary to maintain the two-dimensional organization of the monolayer. Thus, our studies show that pp60$^{c\text{-}src}$ has the biological potential to modulate the spatial organization of epithelial cells during epithelial morphogenesis.

Does the pp60$^{c\text{-}src}$-induced trait in MDCK cells represent a natural function of pp60$^{c\text{-}src}$? A consideration of the expression of pp60$^{c\text{-}src}$ in development and evolution may provide clues about the function of pp60$^{c\text{-}src}$. Low levels of pp60$^{c\text{-}src}$ or c-*src* RNA have been detected in nearly all vertebrate cells and tissues examined, but a few specialized types of cells express much greater levels of pp60$^{c\text{-}src}$ than other cell types (27, 37, 55, 60). In the developing central nervous system, a large increase in pp60$^{c\text{-}src}$ expression occurs at the onset of neuronal differentiation (15, 21, 45, 47, 48, 64, 71). pp60$^{c\text{-}src}$ levels are highest in certain postmitotic neurons undergoing dynamic changes in their spatial organization, such as the neuroepithelial cells that form the folding edge of the developing neural tube (48) and tracts of growing axonal processes in the developing retina and cerebellum (21, 64). Regions of the developing insect nervous system exhibit a similar enrichment of c-*src* transcripts (62). In addition, platelet membranes (25) and monocytic leukocytes and macrophages express elevated levels of pp60$^{c\text{-}src}$ (2, 22, 27).

Differentiating neurons, mature platelets, and monocyte-macrophages appear to share few characteristics since they exhibit widely divergent differentiated features. However, these types of cells lack proliferative potential and can be distinguished from types of cells which express low levels of pp60$^{c\text{-}src}$ by their characteristic ability to undergo marked changes in cell shape. Differentiating postmitotic neurons engage in diverse morphogenetic movements such as neurite outgrowth, neuroepithelial folding, and cell migration (1, 20, 31, 69). Activated platelets rapidly change their rigid, discoid shapes into highly distorted forms that make up the platelet (hemostatic) plug (19, 76). Monocyte-macrophages exhibit extreme structural plasticity during diapedesis, chemotaxis, and phagocytosis (12, 16, 77). The pp60$^{c\text{-}src}$ protein may perform a fundamental physiological action in most or all higher eucaryotic cells, because of its high degree of evolutionary conservation and its widespread expression in animal cells and tissues. However, the fact that pp60$^{c\text{-}src}$ becomes expressed at particularly high levels in types of cells which characteristically undergo marked changes in cell shape raises the possibility that pp60$^{c\text{-}src}$ plays a role in the regulation of the structural plasticity and hence shape of cells.

Our experiments demonstrated a biological activity of pp60$^{c\text{-}src}$ that fits well with these limited predictions about the natural function of pp60$^{c\text{-}src}$. Elevated levels of pp60$^{c\text{-}src}$ were not mitogenic and selectively induced a high degree of structural plasticity in MDCK cells. Significantly, elevated levels of pp60$^{c\text{-}src}$ did not disturb the specific differentiated morphological features of MDCK cells, since these cells established normal morphological polarity and exhibited no detectable alteration of their specific epithelial cell-cell contacts. We suggest that a natural function of the cellular tyrosine kinase, pp60$^{c\text{-}src}$, is to induce structural plasticity in cells and multicellular structures undergoing dynamic changes in spatial organization.

ACKNOWLEDGMENTS

We are grateful to Sally Shephardson for processing the cells for electron microscopy and to Annmarie Shepherd, Donna Hnosko, and Gloria Szymanski for typing the manuscript. We thank Jesse Summers and Russell Lebovitz for their comments on the manuscript. We also thank Joan Brugge for MAb 327, Barry Gumbiner for the rr-1 antibody, Hidesaburo Hanafusa for the p5H plasmid, Carl-Henrik Heldin for the antiphosphotyrosine antibodies, Robert Perry for ribosomal protein 32, and David Shalloway for the pMv-*src* plasmid.

This work was supported in part by Public Health Service grant (GM-35527) from the National Institutes of Health to W.J.N. and by a grant from the National Science Foundation to W.J.N. (DCB-8609091). S.L.W. was supported by a postdoctoral fellowship (CA0-07638) from the National Institutes of Health.

LITERATURE CITED

1. **Arey, L. B.** 1946. Developmental anatomy, 5th ed., p. 413–477. The W. B. Saunders Co., Philadelphia.
2. **Barnekow, A., and M. Gessler.** 1986. Activation of the pp60$^{c\text{-}src}$ kinase during differentiation of monomyelocytic cells *in vitro*. EMBO J. **5**:701–705.
3. **Bernfield, M. R., and N. K. Wessels.** 1970. Intra- and extracellular control of epithelial morphogenesis. Dev. Biol. **4**(Suppl.): 195–249.
4. **Bishop, J. M.** 1983. Cellular oncogenes and retroviruses. Annu. Rev. Biochem. **52**:301–354.
5. **Brugge, J. S., and R. L. Erikson.** 1977. Identification of a transformation-specific antigen induced by avian sarcoma virus. Nature (London) **269**:346–348.
6. **Brugge, J. S., E. Erikson, and R. L. Erikson.** 1978. Antibody to virion structural proteins in mammals bearing avian sarcoma virus-induced tumors. Virology **84**:429–433.
7. **Brugge, J. S., P. C. Cotton, A. E. Queral, J. N. Barrett, D. Nonner, and R. W. Keane.** 1985. Neurones express high levels of a structurally modified, activated form of pp60$^{c\text{-}src}$. Nature (London) **316**:554–557.
8. **Burgess, D. R.** 1982. Reactivation of intestinal epithelial cell brush border motility. ATP-dependent contraction via a terminal web contractile ring. J. Cell Biol. **95**:853–866.
9. **Cartwright, C. A., W. Eckhart, S. Simon, and P. L. Kaplan.** 1987. Cell transformation by pp60$^{c\text{-}src}$ mutated in the carboxy-terminal regulatory domain. Cell **49**:83–91.
10. **Cereijido, M., J. Ehrenfeld, I. Meza, and A. Martinez-Palomo.** 1980. Structural and functional membrane polarity in cultured monolayers of MDCK cells. J. Membr. Biol. **52**:147–159.
11. **Cereijido, M., E. S. Robbins, W. J. Dolan, C. A. Rotonno, and D. D. Sabatini.** 1978. Polarized monolayers formed by epithelial cells on a permeable and translucent support. J. Cell Biol. **77**: 853–880.
12. **Cohn, Z. A., and B. Benson.** 1964. The differentiation of

mononuclear phagocytes: morphology, cytochemistry and biochemistry. J. Exp. Med. **121**:153–170.
13. **Collett, M. S., and R. L. Erikson.** 1978. Protein kinase activity associated with the avian sarcoma virus *src* gene product. Proc. Natl. Acad. Sci. USA **75**:2021–2024.
14. **Cone, R. D., and R. C. Mulligan.** 1984. High-efficiency gene transfer into mammalian cells: generation of helper-free recombinant retrovirus with broad mammalian host range. Proc. Natl. Acad. Sci. USA **81**:6349–6353.
15. **Cotton, P. C., and J. S. Brugge.** 1983. Neural tissues express high levels of the cellular *src* gene product, pp60$^{c\text{-}src}$. Mol. Cell. Biol. **3**:1157–1162.
16. **Ebert, R. H., and H. W. Florey.** 1939. The extravascular development of the monocyte observed *in vivo*. Br. J. Exp. Pathol. **20**:342–345.
17. **Ek, B., and C.-H. Heldin.** 1984. Use of an antiserum against phosphotyrosine for the identification of phosphorylated components in human fibroblasts stimulated by platelet-derived growth factor. J. Biol. Chem. **259**:11145–11152.
18. **Farquhar, M. G., and G. E. Palade.** 1963. Junctional complexes in various epithelia. J. Cell Biol. **17**:375–412.
19. **French, J. E., R. G. MacFarlane, and A. G. Saunders.** 1964. The structure of hemostatic plugs and experimental thrombi in small arteries. Br. J. Exp. Pathol. **45**:467–474.
20. **Fujita, S.** 1964. Analysis of neuron differentiation in the central nervous system by tritiated thymidine autoradiography. J. Comp. Neurol. **112**:311–327.
21. **Fults, D. W., A. C. Towle, J. M. Lauder, and P. F. Maness.** 1985. pp60$^{c\text{-}src}$ in developing cerebellum. Mol. Cell. Biol. **5**:27–32.
22. **Gee, C. E., J. Griffin, L. Sastre, L. J. Miller, T. A. Springer, H. Piwnica-Worms, and T. M. Roberts.** 1986. Differentiation of myeloid cells is accompanied by increased levels of pp60$^{c\text{-}src}$ protein and kinase activity. Proc. Natl. Acad. Sci. USA **83**: 5131–5135.
23. **Geiger, B., Z. Avnur, G. Rinnerthaler, H. Hinssen, and V. I. Small.** 1984. Microfilament organizing centers in areas of cell contact: cytoskeletal interactions during attachment and locomotion. J. Cell Biol. **99**:83s–91s.
24. **Geiger, B., A. H. Dutton, K. T. Tokuyasu, and S. J. Singer.** 1981. Immunoelectron microscopic studies of membrane-microfilament interaction. The distribution of α-actinin, tropomyosin and vinculin in intestinal epithelial brush border and in chicken gizzard smooth muscle. J. Cell Biol. **91**:614–628.
25. **Geldin, A., S. P. Nemeth, and J. S. Brugge.** 1986. Blood platelets express high levels of the pp60$^{c\text{-}src}$ specific tyrosine kinase activity. Proc. Natl. Acad. Sci USA **83**:852–857.
26. **Gilead, Z., Y.-H. Jeng, W. S. M. Wold, K. Sugawara, H. M. Rho, M. L. Harter, and M. Green.** 1976. Immunological identification of two adenovirus 2-induced early proteins possibly involved in cell transformation. Nature (London) **264**:263–266.
27. **Gonda, T. J., D. K. Sheiness, and J. M. Bishop.** 1982. Transcripts from cellular homologs of retroviral oncogenes, distribution among chicken tissues. Mol. Cell. Biol. **2**:617–624.
28. **Grobstein, C.** 1955. Inductive interactions in the mouse metanephros. J. Exp. Zool. **130**:319–329.
29. **Gumbiner, B., and K. Simons.** 1986. A functional assay for proteins involved in establishing an epithelial occluding barrier: identification of a uvomorulin-like polypeptide. J. Cell Biol. **102**:457–468.
30. **Hall, H. G., D. A. Farson, and M. J. Bissel.** 1982. Lumen formation by epithelial cell lines in response to collagen overlay: a morphogenetic model in culture. Proc. Natl. Acad. Sci. USA **79**:4672–4676.
31. **Harrison, R. G.** 1910. The outgrowth of the nerve fiber as a mode of protoplasmic movement. J. Exp. Zool. **9**:787–848.
32. **Heath, J. P., and G. A. Dunn.** 1978. Cell to substratum contacts of chick fibroblasts and their relation to the microfilament system. A correlated interface-reflexion and high voltage electron-microscopic study. J. Cell Sci. **29**:197–212.
33. **Hilfer, R. S., B. Y. Palmatier, and E. M. Fithian.** 1977. Precocious evagination of embryonic chick thyroid in ATP-containing medium. J. Embryol. Exp. Morphol. **42**:163–175.
34. **Hunter, T.** 1987. A tail of two *src*'s: mutatis mutandis. Cell **49**:1–4.
35. **Hunter, T., and J. A. Cooper.** 1985. Protein-tyrosine kinases. Annu. Rev. Biochem. **54**:897–930.
36. **Iba, M., T. Takeya, F. R. Cross, T. Hanafusa, and M. Hanafusa.** 1984. Rous sarcoma virus variants that carry the cellular *src* gene instead of the viral *src* gene cannot transform chicken embryo fibroblasts. Proc. Natl. Acad. Sci. USA **79**:4628–4632.
37. **Jacobs, C., and H. Rubsamen.** 1983. Expression of pp60$^{c\text{-}src}$ protein kinase in adult and fetal human tissue: high activities in some sarcomas and mammary carcinomas. Cancer Res. **43**: 1692–1702.
38. **Johnson, P. J., P. M. Coussens, A. V. Danko, and D. Shalloway.** 1985. Overexpression of pp60$^{c\text{-}src}$ can induce focus formation without complete transformation of NIH 3T3 cells. Mol. Cell. Biol. **5**:1073–1083.
39. **Karfunkel, P.** 1974. The mechanisms of neural tube formation. Int. Rev. Cytol. **38**:245–271.
40. **Keller, T. C. S., and M. S. Mooseker.** 1982. Ca^{++} calmodulin-dependent phosphorylation of myosin, and its role in brush border contraction *in vitro*. J. Cell Biol. **95**:943–959.
41. **Kmiecik, T. E., and D. Shalloway.** 1987. Activation and suppression of pp60$^{c\text{-}src}$ transforming ability by mutation of its primary sites of tyrosine phosphorylation. Cell **49**:65–73.
42. **Kriegler, M., C. F. Perez, C. Hardy, and M. Botchan.** 1984. Transformation mediated by the SV40 T antigen: separation of the overlapping SV40 early genes by a retroviral vector. Cell **38**: 483–491.
43. **Laemlli, U. K.** 1970. Cleavage of structural proteins during the assembly of the head of bacteriophage T4. Nature (London) **227**:680–685.
44. **Levy, J. B., H. Iba, and H. Hanafusa.** 1986. Activation of the transforming potential of pp60$^{c\text{-}src}$ by a single amino acid change. Proc. Natl. Acad. Sci. USA **83**:4228–4232.
45. **Levy, B. T., L. K. Sorge, A. Meymandi, and P. F. Maness.** 1984. pp60$^{c\text{-}src}$ kinase is in chick and human embryonic tissues. Dev. Biol. **104**:9–17.
46. **Lipisch, L. A., A. J. Lewis, and J. S. Brugge.** 1983. Isolation of monoclonal antibodies that recognize the transforming proteins of avian sarcoma viruses. J. Virol. **48**:352–360.
47. **Lynch, S. A., J. S. Brugge, and J. M. Levine.** 1986. Induction of altered c-*src* product during neural differentiation of embryonal carcinoma cells. Science **234**:873–876.
48. **Maness, P. F., L. K. Sorge, and D. W. Fults.** 1986. An early developmental phase of pp60$^{c\text{-}src}$ expression in the neural ectoderm. Dev. Biol. **117**:83–89.
49. **Maniatis, T., E. F. Fritsch, and J. Sambrook.** 1982. Molecular cloning: a laboratory manual. Cold Spring Harbor Laboratory, Cold Spring Harbor, N.Y.
50. **Mann, R., R. C. Mulligan, and D. B. Baltimore.** 1983. Construction of a retrovirus packaging mutant and its use to produce helper-free defective retrovirus. Cell **33**:153–159.
51. **Marchesi, V. T.** 1985. Stabilizing infrastructure of cell membranes. Annu. Rev. Cell Biol. **1**:531–561.
52. **Misfeldt, D. S., S. T. Hammanmoka, and D. R. Pitelka.** 1976. Transepithelial transport in cell culture. Proc. Natl. Acad. Sci. USA **73**:1212–1215.
53. **Mooseker, M. S.** 1985. Organization, chemistry and assembly of the cytoskeletal apparatus of the intestinal brush border. Annu. Rev. Cell Biol. **1**:209–241.
54. **Nelson, W. J., and P. Veshnock.** 1986. Dynamics of membrane-skeleton (fodrin) organization during development of polarity in Madin-Darby canine kidney (MDCK) epithelial cells. J. Cell Biol. **103**:1751–1765.
55. **Oppermann, H., A. D. Levinson, H. E. Varmus, L. Levintow, and J. M. Bishop.** 1979. Uninfected vertebrate cells contain a protein that is closely related to the product of the avian sarcoma virus transforming gene (*src*). Proc. Natl. Acad. Sci. USA **76**:1804–1808.
56. **Parker, R. C., H. E. Varmus, and J. M. Bishop.** 1984. Expression of v-*src* and chicken c-*src* in rat cells demonstrates qualitative differences between pp60$^{v\text{-}src}$ and pp60$^{c\text{-}src}$. Cell **37**:131–139.
57. **Piwnica-Worms, H., K. B. Saunders, T. M. Roberts, A. E.**

Smith, and S. H. Cheng. 1987. Tyrosine phosphorylation regulates the biochemical and biological properties of pp60$^{c\text{-}src}$. Cell **49**:75–82.
58. **Rodewald, R. S., S. B. Newman, and M. J. Karnovsky.** 1976. Contraction of isolated brush borders from the intestinal epithelium. J. Cell Biol. **70**:541–554.
59. **Saier, M. H.** 1981. Growth and differentiation properties of a kidney epithelial cell line (MDCK). Am. J. Physiol. **240**:C106–C109.
60. **Schartl, M., and A. Barnekow.** 1982. The expression in eukaryotes of a tyrosine kinase which is reactive with pp60$^{v\text{-}src}$ antibodies. Differentiation **23**:109–114.
61. **Shalloway, D., P. M. Coussens, and P. Yaciuk.** 1984. Overexpression of the c-*src* protein does not induce transformation of NIH 3T3 cells. Proc. Natl. Acad. Sci. USA **81**:7071–7075.
62. **Simon, M. A., B. Drees, T. Kornberg, and J. M. Bishop.** 1985. The nucleotide sequence and the tissue-specific expression of Drosophila c-*src*. Cell **42**:831–840.
63. **Simons, K., and S. D. Fuller.** 1985. Cell surface polarity in epithelia. Annu. Rev. Cell Biol. **1**:243–288.
64. **Sorge, L. K., B. T. Levy, and P. F. Maness.** 1984. pp60$^{c\text{-}src}$ is developmentally regulated in the neural retina. Cell **36**:249–257.
65. **Spooner, B. S., and N. K. Wessels.** 1972. An analysis of salivary gland morphogenesis: role of cytoplasmic microfilaments and microtubules. Dev. Biol. **27**:38–54.
66. **Swanstrom, R., R. C. Parker, H. E. Varmus, and J. M. Bishop.** 1983. Transduction of a cellular oncogene: the genesis of Rous sarcoma virus. Proc. Natl. Acad. Sci. USA **80**:2519–2524.
67. **Takeya, T., and H. Hanafusa.** 1983. Structure and sequence of the cellular gene homologous to the RSV *src* gene and the mechanism for generating the transforming virus. Cell **32**:881–890.
68. **Trinkaus, J. P.** 1984. Cells into organs. Prentice-Hall, Inc., Englewood Cliffs, N.J.
69. **Truex, R. C., and M. B. Carpenter.** 1969. Human neuroanatomy, 6th ed. The Williams & Wilkins Co., Baltimore.
70. **Valentich, J. D., R. Tchao, and J. Leighton.** 1979. Hemicyst formation stimulated by cyclic AMP in dog kidney cell line MDCK. J. Cell Physiol. **100**:291–304.
71. **Vardimon, L., L. E. Fox, and A. A. Moscona.** 1986. Accumulation of c-*src* mRNA is developmentally regulated in embryonic neural retina. Mol. Cell. Biol. **6**:4109–4116.
72. **Warren, S. L., and W. J. Nelson.** 1987. Nonmitogenic morphoregulatory action of pp60$^{v\text{-}src}$ on multicellular epithelial structures. Mol. Cell. Biol. **7**:1326–1337.
73. **Weeds, A.** 1982. Actin-binding proteins: regulators of cell architecture and motility. Nature (London) **296**:811–816.
74. **Wehland, J., M. Osborn, and K. Weber.** 1979. Cell to substratum contacts in living cells, a direct correlation between interference-reflexion and indirect immunofluorescence microscopy using antibodies against actin and α-actinin. J. Cell Sci. **37**:257–273.
75. **Wessels, N. K., B. S. Spooner, J. F. Ash, M. O. Bradley, M. A. Ludena, E. L. Taylor, J. T. Wrenn, and K. M. Yamada.** 1971. Microfilaments in cellular and developmental processes. Science **171**:135–143.
76. **Zuker, M. B.** 1980. The functioning of blood platelets. Sci. Am. **242**:86–103.
77. **Zukerman, S. H., and S. D. Douglas.** 1979. Dynamics of the macrophage plasma membrane. Annu. Rev. Microbiol. **33**:267–307.